Insulin-like Growth Factor Receptor as a Therapeutic Target in Head and Neck Cancer

Christopher J. Barnes,[1] Kazufumi Ohshiro,[1] Suresh K. Rayala,[1] Adel K. El-Naggar,[2] and Rakesh Kumar[1,3]

Abstract

Purpose: Insulin-like growth factor type I receptor (IGF-IR) plays critical roles in epithelial cancer cell development, proliferation, motility, and survival, and new therapeutic agents targeting IGF-IR are in development. Another receptor tyrosine kinase, the epidermal growth factor receptor (EGFR), is an established therapeutic target in head and neck cancer and IGF-IR/EGFR heterodimerization has been reported in other epithelial cancers. The present study was undertaken to determine the effects of anti – IGF-IR therapeutic targeting on cell signaling and cancer cell phenotypes in squamous cell carcinomas of the head and neck (SCCHN).

Experimental Design: The therapeutic efficacy of the human anti – IGF-IR antibody IMC-A12 alone and in combination with the EGFR blocking antibody cetuximab (C225) was tested in SCCHN cell lines and in tumor xenografts.

Results: IGF-IR was overexpressed in human head and neck cancer cell lines and tumors. Pretreatment of serum-starved 183A or TU159 SCCHN cell lines with A12 (10 μg/mL) blocked IGF-stimulated activation of IGF-IR, insulin receptor substrate (IRS) -1 and IRS-2, mitogen-activated protein kinase, and phosphatidylinositol 3-kinase. A12 induced G_0-G_1 cell cycle arrest and blocked cell growth, motility, and anchorage-independent growth. Stimulation of head and neck cancer cells with either IGF or EGF resulted in IGF-IR and EGFR heterodimerization, but only IGF caused activating phosphorylation of both receptors. Combined treatment with A12 and the EGFR blocking antibody C225 was more effective at reducing cell proliferation and migration than either agent alone. Finally, TU159 tongue cancer cell xenografts grown in athymic nude mice were treated thrice weekly for 4 weeks with vehicle, A12 (40 mg/kg i.p.), C225 (40 mg/kg i.p.), or both agents (n = 8 mice per group; 2 tumors per mouse). Linear regression slope analysis showed significant differences in median tumor volume over time between all three treatment groups and the control group. Complete regression was seen in 31% (A12), 31% (C225), and 44% (A12 + C225) of tumors.

Conclusion: Here we found the overexpression of IGF-IR, the functional heterodimerization of IGF-IR and EGFR, and effective therapeutic targeting of these receptors in human head and neck cancer xenografts.

Squamous cell carcinoma of the head and neck (SCCHN) is the fifth most common cancer worldwide and is a significant source of cancer morbidity and mortality in the United States (1). Despite decades of research and treatment advances, there has been little improvement in patient 5-year survival rates, with local recurrence, second primary cancers, and local and distant metastases remaining significant barriers to disease eradication. Recent advances in molecularly targeted cancer therapeutics have shown some early success. One such target is the epidermal growth factor (EGF) receptor (EGFR), which is highly expressed in 40% to 90% of human SCCHN (2). Systemically circulating and locally produced ligands such as transforming growth factor-α activate EGFR and initiate intracellular signaling cascades. This signaling leads to increased cell proliferation, resistance to apoptotic stimuli, enhanced cell motility, and local production of angiogenic factors (2). Blockade of EGFR signaling via systemic administration of blocking antibodies or small-molecule receptor tyrosine kinase inhibitors has been shown to effectively reduce SCCHN aggressive cell phenotypes, block angiogenesis, and induce cancer cell death, but long-term follow up data are currently lacking and these agents have proved effective only in subsets of patients (3).

A newly emerging target for cancer chemotherapy is the insulin-like growth factor (IGF) signaling axis. Both preclinical research and clinical investigations have implicated the IGF type I receptor (IGF-IR) and its ligands IGF-I and IGF-II in the development and progression of a number of human cancers (4 – 6). Increases in systemically circulating IGF-1 levels and

Authors' Affiliations: Departments of [1]Molecular and Cellular Oncology and [2]Pathology, The University of Texas M. D. Anderson Cancer Center, and [3]Molecular and Cellular Biology, Baylor College of Medicine, Houston, Texas

Received 8/18/06; revised 4/6/07; accepted 5/9/07.

Grant support: NIH Specialized Program of Research Excellence grants 5P50 CA097007 and CA65746 (R. Kumar).

The costs of publication of this article were defrayed in part by the payment of page charges. This article must therefore be hereby marked *advertisement* in accordance with 18 U.S.C. Section 1734 solely to indicate this fact.

Note: Supplementary data for this article is available at Clinical Cancer Research Online (http://clincancerres.aacrjournals.org/).

Requests for reprints: Rakesh Kumar, University of Texas M. D. Anderson Cancer Center, Houston, TX 77030. Phone: 713-745-3559; Fax: 713-794-0209; E-mail: rkumar@mdanderson.org.

doi:10.1158/1078-0432.CCR-06-2040

elevated tissue IGF-IR expression are associated with increased risk of numerous cancer types and more rapid disease progression (4). The binding of IGF-I or IGF-II to the IGF-IR initiates conformational changes in this tetramer transmembrane receptor tyrosine kinase that initiate autophosphorylation and subsequent activation of Ras-Raf-mitogen-activated protein kinase and phosphatidylinositol 3-kinase-protein kinase B/AKT signaling cascades. IGF-IR can stimulate a wide variety of responses in cells, including cell proliferation, cell differentiation, changes in cell size, cell adhesion and motility, and resistance to apoptotic stimuli. High expression of IGFs and IGF-IR has also been associated with tumor metastatic potential (7–9). Furthermore, overexpression of a constitutively active IGF-IR in the mouse mammary gland is sufficient for tumorigenesis (10), whereas expression of a dominant negative IGF-IR blocked cell transformation by Ras (11).

The fundamental role of IGF-IR as a cell survival factor has been shown in a variety of cell types and IGF-IR expression is inversely related to susceptibility to apoptosis (12). The proliferative and antiapoptotic effects of IGF-IR signaling are mediated through an adaptor protein called insulin receptor substrate 1 (IRS-1), which functions as a scaffold protein and facilitates the activation of a number of signaling molecules (4, 5). The adaptor protein IRS-2 is also activated by IGF-IR tyrosine kinase activity. On activation, IRS-2 facilitates focal adhesion kinase phosphorylation, dissolution of both focal adhesions and actin stress fibers, and enhanced cell motility (13). Along these lines, stable expression of a dominant negative IGF-IR blocked the ability of breast cancer xenografts to metastasize (14). IGF-IR has also been shown to directly interact with β_1 integrin complexes (15). Thus, there may be a regulatory link between IGF-IR, specific integrin-mediated focal adhesion complexes, and the regulation of cell motility and invasion.

To date, there are no studies investigating the expression or function of IGF-IR in human head and neck cancer. Given the integral role of this signaling axis in organismal development, cell regulation, and cancer development and progression in other disease settings, we recently initiated studies into the expression and biological significance of IGF-IR in head and neck cancer.

Materials and Methods

Cell culture and reagents. The human head and neck cancer cell lines TU159, 183A, and 1483 (16) were provided by Reuben Lotan (M.D. Anderson Cancer Center, Houston, TX) and all others were from the laboratory of Gary Glayman (M.D. Anderson Cancer Center, Houston, TX). All cells were grown in DMEM/F-12 nutrient mixture (1:1) supplemented with 10% FCS. Specific antibodies against the following antigens were used: phospho-p42/p44 extracellular signal–regulated kinase (ERK), phospho-S473 AKT, phospho-Y1086 EGFR (Cell Signaling Technology); IGF-IRα (3B7), IGF-IRβ (C20), ERK2 (Santa Cruz Biotechnology); phospho-Y1158/1162/1163 IGF-IR, phospho-Y612 IRS-1, phospho-S731 IRS-2 (Biosource International); and vinculin (Sigma Chemical Co.). Antimouse and antirabbit horseradish peroxidase conjugates were from Amersham. Antibody against proliferating cell nuclear antigen (PCNA) was purchased from Genetex. Human recombinant IGF and EGF were purchased from Calbiochem. The therapeutic monoclonal antibodies IMC-A12 and C225 (cetuximab, Erbitux) were kindly provided by ImClone Systems, Inc. In all experiments, analytic or reagent grade products were used without further purification.

Cell culture, reporter assay, cell growth, and RNA interference. Cell lines were maintained in DMEM/F-12 (1:1) supplemented with 10% FCS. For cell growth assays, cells were grown in six-well plates and treated as described. Cells were trypsinized and counted with a Coulter counter at the indicated times. Alternatively, cells were seeded (10,000 per well) in 96-well plates, treated as described, and then subjected to tetrazolium dye 3-(4,5-dimethylthiazol-2-yl)-2,5-diphenyltetrazolium bromide cell viability assays as previously described (17). RNA interference transfections were done using OligofectAMINE (Invitrogen) according to the manufacturer's protocol. A pool of four target verified individual siRNA oligos directed against IGF-IR was purchased from Dharmacon. Seventy-two hours was allowed to elapse after transfection to allow efficient silencing of the gene. The selectivity of IGF-IR knockdown was evaluated by Western blot.

Cell extracts, immunoblotting, and immunoprecipitation. To prepare cell extracts, cells were washed thrice with PBS and then lysed in NP40 lysis buffer [50 mmol/L Tris-HCl (pH 8.0), 137 mmol/L NaCl, 10% glycerol, 1% NP40, 50 mmol/L NaF, 1× protease inhibitor mixture (Roche Biochemical), and 1 mmol/L sodium vanadate] for 15 min on ice. The lysates were centrifuged in an Eppendorf centrifuge at 4°C for 15 min. Cell lysates containing equal amounts of protein (~100 μg) were resolved on SDS-polyacrylamide gels (8-10% acrylamide), transferred to nitrocellulose membranes, probed with the appropriate antibodies, and developed using the enhanced chemiluminescence method (Amersham). For immunoprecipitation, cells were lysed in 50 mmol/L Tris-HCl (pH 8.0), 500 mmol/L NaCl, 3 mmol/L $MgCl_2$. Equal amounts of protein (1 mg, max 200 μL) were diluted to a final volume of 1 mL with 50 mmol/L Tris-HCl (pH 8.0), 3 mmol/L $MgCl_2$ to adjust the final concentration of NaCl to 100 mmol/L. Immunoprecipitation with either a mouse immunoglobulin G antibody or an anti–IGF-IR antibody (3B7, Santa Cruz Biotechnology) was then done overnight at 4°C using 1 μg antibody/mg protein. After extensive washing in 20 mmol/L Tris-HCl (pH 8.0) with 50 mmol/L NaCl and 1 mmol/L EDTA, proteins were detected as described above.

Immunofluorescent labeling and confocal microscopy. The cellular localization of proteins of interest was accomplished by indirect immunofluorescence as previously described (18). Briefly, TU159 cells were plated on sterile glass coverslips in six-well plates and allowed to attach overnight. Following appropriate experimental treatments, cells were rinsed twice in PBS, fixed in 4% phosphate-buffered paraformaldehyde for 15 min, and permeabilized in acetone at -20°C for 4 min. Following permeabilization, cells were blocked in 5% normal goat serum-PBS for 30 min, incubated with a primary antibody against IGF-IR for 1 h at room temperature, washed thrice in PBS, and then incubated with goat anti-mouse secondary antibodies conjugated with Alexa Fluor 488 (green; Molecular Probes). Finally, cells were counterstained with Alexa Fluor 546 (red)–conjugated phalloidin (for detecting F-actin) and the DNA dye Topro-3 (blue; Molecular Probes). Microscopic analyses were done using an Olympus FV300 laser scanning confocal microscope in accordance with established methods, using sequential laser excitation to minimize the possibility of fluorescence emission bleed through. Each image is a single Z section at the same cellular level and magnification.

Wound healing assay. Cell migration potential was also assessed using an established wound healing assay as previously described (19). Briefly, 183A or TU159 cells were plated onto 60-mm dishes in 10% FCS-DMEM. When cells were 80% to 90% confluent, they were rinsed twice in PBS, then cultured in serum-free DMEM for 24 h. The confluent monolayer of cells was then wounded by scraping a narrow 200-mL pipetman tip across the plate in six parallel lines. Cells were rinsed twice in PBS and wound widths were measured by phase-contrast microscopy using Zeiss Axiovision 3.1 software. Cells were then grown in 0% DMEM or medium supplemented with the agents IGF (10 ng/mL), A12 (10 μg/mL), and/or C225 (100 nmol/L). After an additional 24 h, each plate was examined again for the amount of wound closure by measuring the physical separation remaining between the original wound widths. Ten separate measurements

were made per plate and each experiment was done in triplicate. Data were expressed as arbitrary units of the mean values (±SD) of three experiments. Data were analyzed using PRISM software (GraphPad Software, Inc.). Analyses included using the Kruskal-Wallis test for overall significant differences followed by Dunn's multiple comparison tests for pair wise analyses of differences within an experiment. Significance was accepted if $P < 0.05$.

Soft-agar and tumorigenicity assays. Soft-agar colony growth assays were done as previously described (20). Briefly, 1 mL of 0.6% Difco agar in DMEM supplemented with 10% fetal bovine serum and insulin was layered onto cell culture plates. Test cells (1×10^4) mixed with 1 mL of 0.36% bactoagar solution in DMEM were layered on top of the 0.6% bactoagar layer. The plates were incubated at 37°C in 5% CO_2 for 21 days.

For tumor xenograft studies, 6- to 8-week-old athymic (*nu/nu*) mice (Charles River Laboratories; eight mice per group) were given bilateral dorsal hind flank injections of TU159 SCCHN cells (1×10^6) suspended in 30% Matrigel in HBSS (Becton Dickinson). Body weights were measured twice weekly before and throughout the experimental period and no significant differences were noted between control and treatment groups (data not shown). Tumor volume was measured with calipers (volume = $L \times w \times w \times 0.52$) and treatment started when tumors were 100 to 200 mm^3. Mice with palpable tumors were randomized into four groups and were given i.p. injections of sterile PBS (vehicle control), C225 (40 mg/kg), A12 (40 mg/kg), or C225 + A12 (40 mg/kg each drug) three times a week for 4 weeks, with tumor volume recorded. At the end of 4 weeks, mice were sacrificed by cervical dislocation and tumors were excised and fixed in 10% buffered formalin. All animal procedures were approved by the institutional animal care and use committee at University of Texas M.D. Anderson Cancer Center (Houston, TX) and were monitored by the institutional veterinary staff.

Formalin-fixed, paraffin-embedded tumor sections were deparaffinized in xylene, rehydrated in graded ethanol, and subjected to routine histologic staining with Mayer's H&E. Stained tumor sections were examined and photomicrographs captured using an Olympus BX51 microscope and Olympus DPManager software. For immunohistochemical detection of PCNA, xenograft sections were deparaffinized with xylene, rehydrated using graded ethanol, incubated in 0.3% H_2O_2 and methanol for 30 min to inactivate endogenous peroxidase, boiled for 20 min in 0.01 mol/L citrate buffer, and cooled for 30 min at room temperature to expose antigenic epitopes. The sections were incubated with 2% normal goat serum in 1% bovine serum albumin and PBS for 30 min and then with anti-PCNA antibodies and incubated overnight at 4°C. The sections were washed thrice with 0.05% Tween in PBS for 10 min, incubated with secondary antibody, developed with 3,3′-diaminobenzidine-H_2O_2, and counterstained with Mayer's hematoxylin. Negative controls were done by replacing the primary antibody with the immunoglobulin G.

Results and Discussion

IGF-IR in head and neck cancer. To establish the expression and importance of IGF-IR in human head and neck cancer, we screened a panel of seven SCCHN cell lines and normal human epidermal keratinocytes for IGF-IR protein expression. We found that five of seven cell lines expressed IGF-IR at varying levels (Fig. 1A). IGF-IR levels were also verified in 12 human head and neck cancers by Western blot (Fig. 1B), with seven tumors showing elevated IGF-IR protein levels compared with paired normal tissue samples (Fig. 1C). These data show for the first time elevated IGF-IR expression in human SCCHN tumors.

We next wished to determine whether IGF-IR expression was important for the growth and/or survival of SCCHN cell lines.

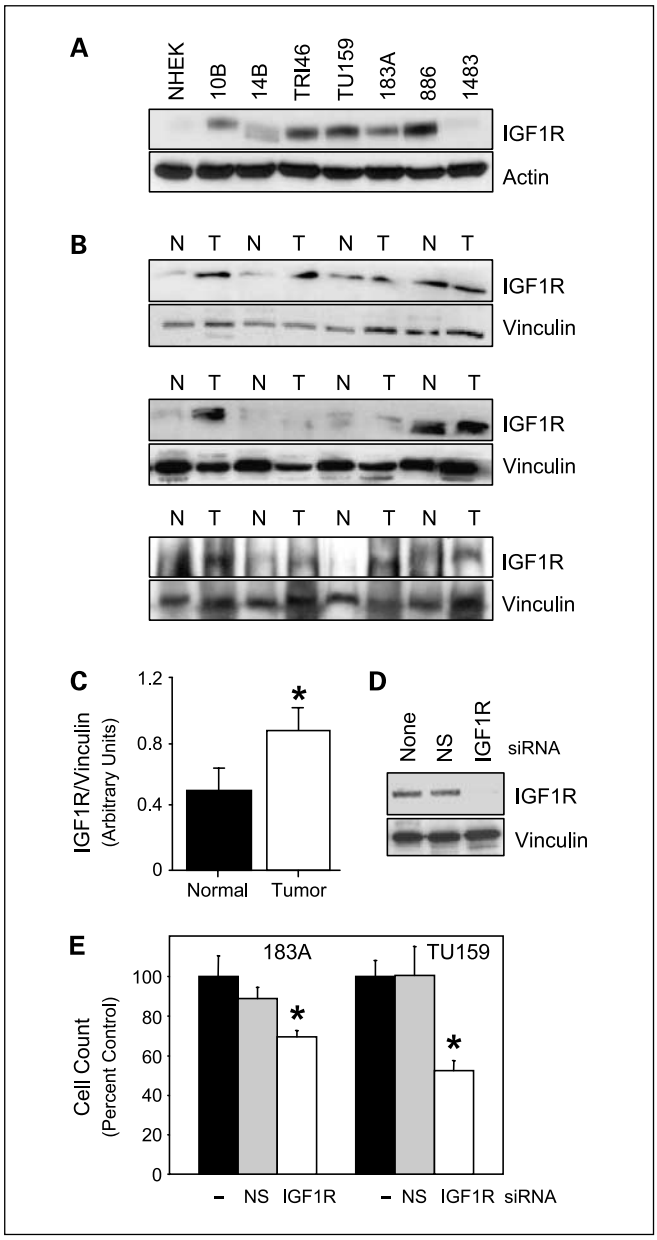

Fig. 1. IGF-IR in human head and neck cancer. *A,* Western blot analysis of IGF-IR and vinculin (as a loading control) in SCCHN cell lines. Western blot analysis (*B*) and scanning densitometry ratios (*C*) of IGF-IR and vinculin expression in paired normal and tumor tissue from tongue cancer patients. *D,* control nonspecific (*NS*) or IGF-IR – specific siRNA was transiently transfected into 183A cells and protein expression was assessed 3 d later by Western blot. *E,* 183A or TU159 cells were transiently transfected with control (nonspecific) or IGF-IR – specific siRNA and total cell counts were assessed 3 d later. *, $P < 0.05$, different from normal tissue (*C*) and the cell line – specific control group (*E*).

Using low (183A) and high (TU159) IGF-IR–expressing cell lines, IGF-IR protein expression was inhibited using IGF-IR–specific siRNA (Fig. 1D). IGF-IR–specific but not control nonspecific siRNA significantly inhibited the growth of these two cell lines (Fig. 1E), although no induction of morphologically evident apoptotic cell death was observed (data not shown).

The anti–IGF-IR therapeutic antibody A12 blocks IGF-induced IGF-IR signaling in SCCHN. Ligand-induced activation of IGF-IR initiates signaling through multiple major mitogenic

and survival pathways, beginning with phosphorylation and activation of the adaptor proteins IRS-1 and IRS-2. IRS-1 and IRS-2 contain conserved pleckstrin homology domains adjacent to a phosphotyrosine binding domain that mediates interaction with the phosphorylated and activated IGF-IR-β subunit. On binding, IRS-1 and IRS-2 become rapidly phosphorylated at multiple sites, triggering conformational changes that facilitate interaction with a number of signaling intermediates and the propagation of signal transduction cascades (21). Increasing recognition of the importance of IGF-IR signaling in the growth and survival of several types of human solid tumors has led to the development of inhibitory agents as novel human cancer therapeutic agents (22). One such agent is the human monoclonal antibody IMC-A12 (A12), which is an effective anticancer therapeutic agent against multiple tumor types in preclinical model systems (23–25).

To determine if IGF-IR activation influenced intracellular signal transduction pathways in SCCHN, 183A cells were grown in complete medium supplemented with 10% FCS or in medium without serum (0%). After 48 h, cells in 0% medium were stimulated with the IGF-IR ligand IGF (10 ng/mL) alone for 10 min, with IGF after 30-min pretreatment with increasing concentration of A12, or with A12 alone (Fig. 2). As expected, IGF treatment rapidly stimulated autophosphorylation of IGF-IR, leading to the phosphorylation of IRS-1. Both these proteins showed decreased phosphorylation as compared with IGF treatment alone when cells were preincubated with A12 (range, 0-10 μg/mL). Thus, A12 effectively blocked the initiation of IGF signaling in 183A cells (Fig. 2 and Suppl. Fig. S1).

We next examined major downstream ERK 1/2 mitogenic and AKT cell survival signaling pathways for activation by IGF and blockade by the A12 monoclonal antibody. ERK 1/2 was phosphorylated following IGF treatment (Fig. 2), but this activation was blocked by pretreatment with A12. AKT showed constitutive phosphorylation on Ser^{473}, which is indicative of activated AKT. This phosphorylation increased slightly after IGF treatment and was slightly inhibited by A12 treatment. The same results were obtained in another SCCHN cells, TU159, except there is no change in the levels of phospho-AKT after A12 treatment (Supplementary Figure). It is interesting to note that these cells did not express detectable levels of phosphatase and tensin homologue (PTEN; data not shown), and a lack of PTEN has been correlated with constitutive AKT activity in head and neck (26, 27) and other solid tumor types. Indeed, constitutive activating phosphorylation of AKT is frequently observed in tongue cancer and other SCCHN (27, 28). Several factors may contribute to constitutive AKT phosphorylation, but loss of PTEN and up-regulation/amplification of PI3K3CA isoform (110α subunit) seem to be mutually exclusive (27).

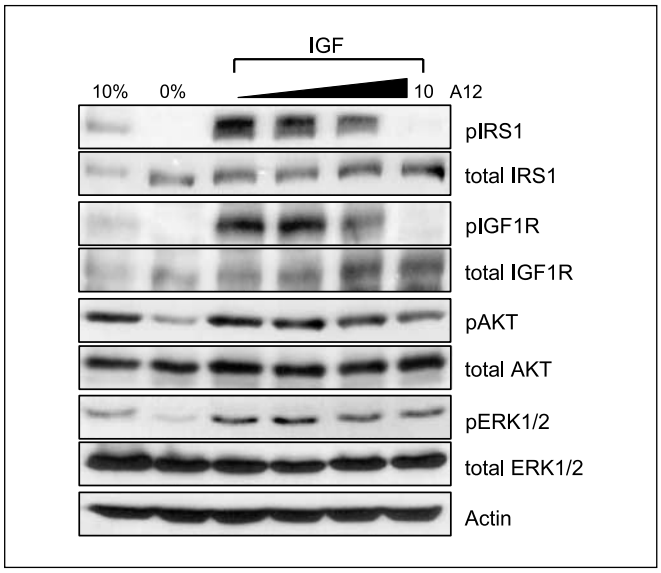

Fig. 2. A12 inhibition of IGF-induced signaling in SCCHN. 183A cells were grown in medium with either 10% or 0% FCS for 48 h, then cells in 0% FCS medium were treated with IGF (10 ng/mL) for 10 min with and without 30 min preincubation with 0, 0.1,1, or 10 μg/mL of the anti – IGF-IR therapeutic antibody A12. Phosphorylation-dependent activation of various signaling molecules was analyzed by Western blot with phosphorylation site – specific antibodies.

A12 blocks cell proliferation and causes G_1 cell cycle arrest in exponentially growing SCCHN cells. Given that IGF-IR knockdown inhibited SCCHN cell proliferation and because the therapeutic antibody A12 effectively blocked IGF-induced mitogenic signaling through IRS-1 and ERK 1/2, we next sought to determine if A12 could affect the growth of exponentially growing SCCHN cells. We found a dose-dependent reduction in the number of viable cells by 3-(4,5-dimethylthiazol-2-yl)-2,5-diphenyltetrazolium bromide assay and in cell proliferation by direct cell counts in cells that were treated with A12 (Fig. 3A and B). These decreases were similar in cell lines expressing low (183A) and high (TU159) levels of IGF-IR, implying the possibility of existence of another independent mechanism. Many antiproliferative agents delay cell cycle progression or induce cell cycle arrest as a means of reducing cell proliferation. To determine if a change in cell cycle distribution might explain the reduced cell growth following A12 treatment, we did fluorescence-activated cell sorting analysis of cells treated with increasing concentrations of A12 (Fig. 3C). We found that A12 induced G_1 cell cycle arrest in TU159 cells (Fig. 3C) and in 183A cells (data not shown). G_1 arrest and inhibition of cell cycle progression following blockade of IGF-IR have been noted in cancer cells from tissues of other origin (22) and in cancer cells treated with other growth factor receptor inhibitors such as the anti-EGFR antibody C225 (29). Thus, IGF-IR inhibition with the blocking antibody A12 induces G_1 cell cycle arrest and seems to be an effective tool for reducing the proliferation of SCCHN.

A12 induces actin stress fibers, blocks cell migration, and inhibits anchorage-independent growth of SCCHN cells. The IGF signaling axis has been shown to be a critical regulator not only of cell proliferation and survival but also of cell motility. Indeed, IGF signaling can influence focal adhesion stability, cell-to-cell contacts, and cell metastasis through its substrate IRS-2 as well as through direct interaction of IGF-IR and integrin complexes in cell focal adhesions (15). Dynamic actin accumulation at the cell periphery is typical of proliferative and motile cells, whereas more static actin structures such as thick actin stress fibers crossing the length of cells are characteristic of growth-inhibited, nonmotile cells (30). To determine if A12 might be inducing actin stress fibers or relocalization of IGF-IR in SCCHN, exponentially growing TU159 cells were treated with A12 (10 μg/mL) for 2 days, then cells were fixed and immunofluorescently labeled for IGF-IR (green), F-actin (red), and DNA (blue). Results indicate that IGF-IR was typically localized at the cell periphery with little F-actin present and mainly at the cell borders (Fig. 4A). However, after A12

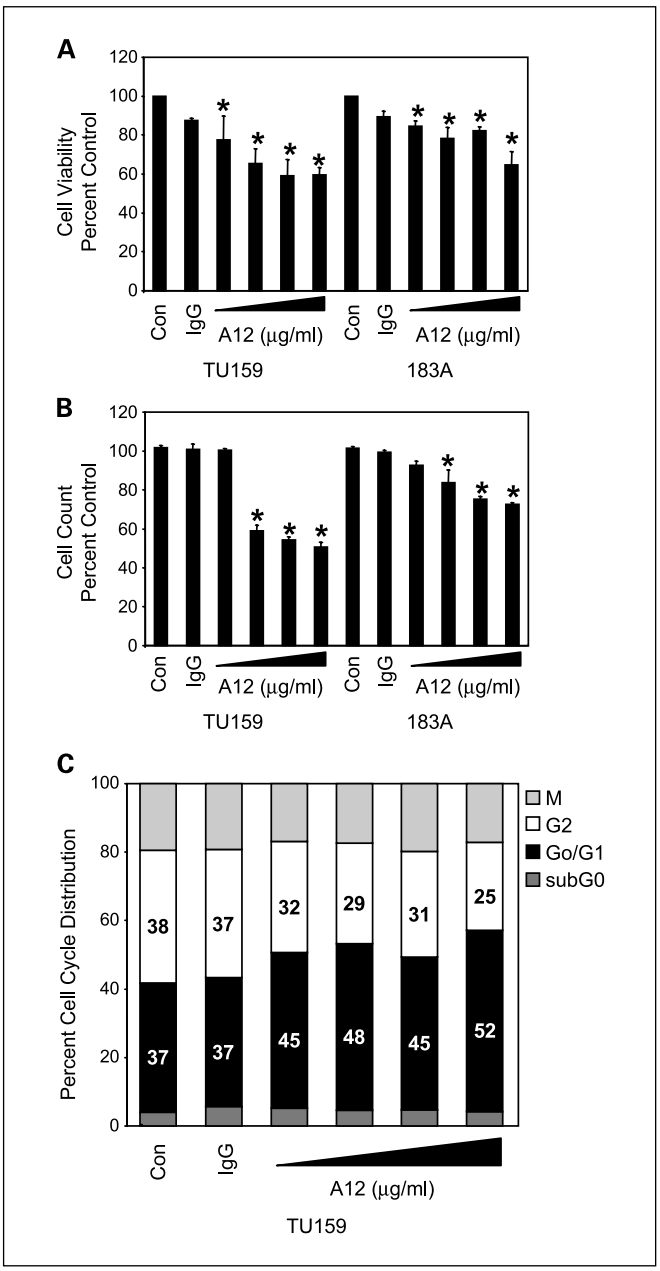

Fig. 3. A12 inhibits cell growth and cell cycle progression in SCCHN. *A* and *B*, TU159 or 183A SCCHN cells grown in medium with 10% FCS were incubated with either immunoglobulin G (*IgG*; 2 μg/mL) or A12 (0.01, 0.1, 1, or 2 μg/mL) for 48 h. Cell viability and growth were assessed by 3-(4,5-dimethylthiazol-2-yl)-2, 5-diphenyltetrazolium bromide assay (*A*) and direct cell counts (*B*), respectively. *C*, cells treated as described above were processed and analyzed by flow cytometry for DNA content and cell cycle distribution. *, $P < 0.05$, different from the cell line – specific control group.

treatment, IGF-IR protein expression was reduced, the receptor was mainly localized to the cell cytoplasm, and cells displayed long, thick fibers of F-actin. These results indicated that A12-treated cells may indeed be less motile. IGF-IR internalization and decreased expression following A12 treatment have also been previously reported (25). Receptor internalization and degradation, in addition to inhibition of signaling, may contribute to the mechanism(s) of action of A12 against SCCHN.

To determine if A12 affected cell motility, 183A and TU159 cells were plated onto cell culture dishes at high density, and when cells became confluent, the cell monolayer was wounded. After baseline wound widths were assessed, cells were incubated in control conditions (no serum), treated with IGF (10 ng/mL), or treated with IGF and A12 (10 μg/mL), and allowed to grow for 24 h. The difference in wound widths from time 0 to 24 h was assessed and it was found that A12 significantly inhibited IGF-induced wound closure (Fig. 4B). These results indicate that IGF induced cell motility in human SCCHN cells and that A12 effectively blocked IGF-induced cell migration.

As an additional test of the ability of A12 to inhibit typical aggressive cancer cell phenotypes, we assessed its influence on anchorage-independent cell growth, an *in vitro* measure of tumorigenicity. Both 183A and TU159 SCCHN cells formed colonies when grown in soft agar, but A12 effectively inhibited colony formation in a dose-dependent manner (Figs. 4C and D). Thus, A12 treatment of SCCHN cells alone inhibited cell cycle progression, mitogenic signaling, cell proliferation, cell motility, and *in vitro* tumorigenicity.

IGF stimulates IGF-IR/EGFR heterodimerization and receptor activation that is sensitive to A12. The frequent requirement of a functional IGF-IR signaling axis for effective EGF mitogenic cell signaling is well established but has taken on new significance with the development of EGFR-directed cancer therapeutics (reviewed in ref. 31). Because EGFR is frequently overexpressed in human head and neck cancer and IGF-IR has been reported to mediate resistance to anti-EGFR–based therapies in other solid tumors (32–34), we decided to test if EGFR and IGF-IR could heterodimerize in SCCHN. We found that when serum-starved TU159 cells were stimulated with either IGF or EGF, EGFR could be immunoprecipitated with an anti–IGF-IR antibody (Fig. 5A). This ligand-stimulated heterodimerization may result in receptor activation because serum-starved TU159 cells showed significant autophosphorylation of EGFR Tyr^{1086} following IGF treatment (Fig. 5B). This activation could be inhibited by preincubation of serum-starved cells with the anti–IGF-IR antibody A12 before ligand treatment. We also wished to see if this ligand-stimulated receptor tyrosine kinase cross talk and activation was bidirectional (i.e., IGF and EGF caused receptor heterodimerization and IGF stimulated EGFR autophosphorylation, but could EGF cause IGF-IR autophosphorylation as a measure of receptor activation). Results indicated that although both IGF and EGF stimulated heterodimerization, IGF-IR was not phosphorylated following EGF treatment (Fig. 5C). As expected, the anti-EGFR antibody C225 reduced EGF-induced EGFR phosphorylation. It is interesting to note that in the squamous carcinoma cell line HN5, which overexpresses EGFR but also expresses IGF-IR, the small-molecule EGFR receptor tyrosine kinase inhibitor erlotinib (OSI-774) was able to block IGF-induced activation of ERK 1/2 signaling but had no effect on AKT activation (34). Thus, some of the downstream signaling effects of IGF-IR activation may rely on EGFR activation.

Because EGFR and IGF-IR regulate overlapping downstream signaling pathways and we were able to detect functional heterodimerization of these two receptors in SCCHN, we next tested the possibility that blocking both of these receptors with therapeutic antibodies may prove more effective than treatment with single agents alone. Results indicate that the combination

of A12 and C225 was more effective than single agents at reducing cell growth (Fig. 5D). Interestingly, the combination of A12 and C225 was only slightly better than A12 alone at reducing IGF-induced cell motility (Fig. 5E); C225 alone was able to significantly reduce the IGF stimulatory effect. These results suggest that, as was reported for ERK activation in HN5 squamous carcinoma cells (35), IGF-induced cell motility may rely, in part, on EGFR activation and/or EGFR-IGF-IR signaling.

EGFR and IGF-IR blocking antibodies, alone and in combination, cause tumor regression in TU159 xenografts. To test the potential therapeutic efficacy of the anti–IGF-IR antibody A12, alone or in combination with the anti-EGFR antibody C225, TU159 cells were grown s.c. in athymic nude mice. Established

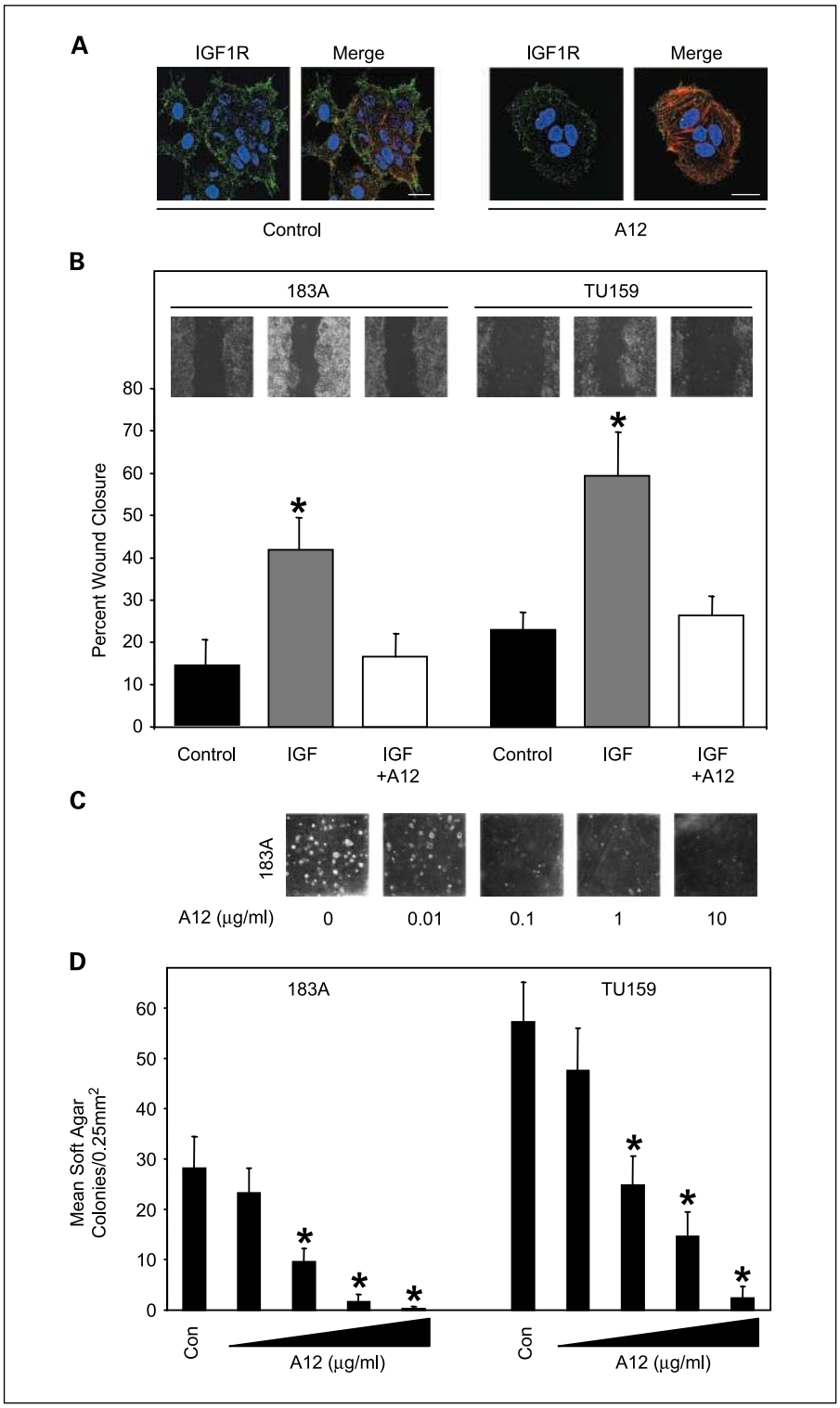

Fig. 4. A12 inhibits malignant phenotypes in SCCHN. *A,* 183A cells were grown on glass coverslips and incubated with either immunoglobulin G (*left*) or A12 (*right*) for 48 h, then cells were fixed and immunofluorescently labeled for IGF-IR (*green*), F-actin (*red*), and DNA (*blue*). Bar, 10 μm. *B,* 183A or TU159 cells were grown to confluency, wounded, and then incubated with IGF alone or IGF plus A12 for 24 h. Each plate was examined by phase-contrast microscopy for the amount of wound closure. Ten separate measurements were made per plate and each experiment was done in triplicate. Columns, mean of three experiments; bars, SD. *C,* representative images of 183A SCCHN soft-agar colony formation. *D,* 183A or TU159 cells were grown in medium with 10% FCS and either 0 (control) or 0.01, 0.1, 1, or 10 μg/mL A12 for 2 wk. Colonies were counted in 10 fields per experiment. Columns, mean of three experiments; bars, SD. *, $P < 0.05$, different from the cell line–specific control group.

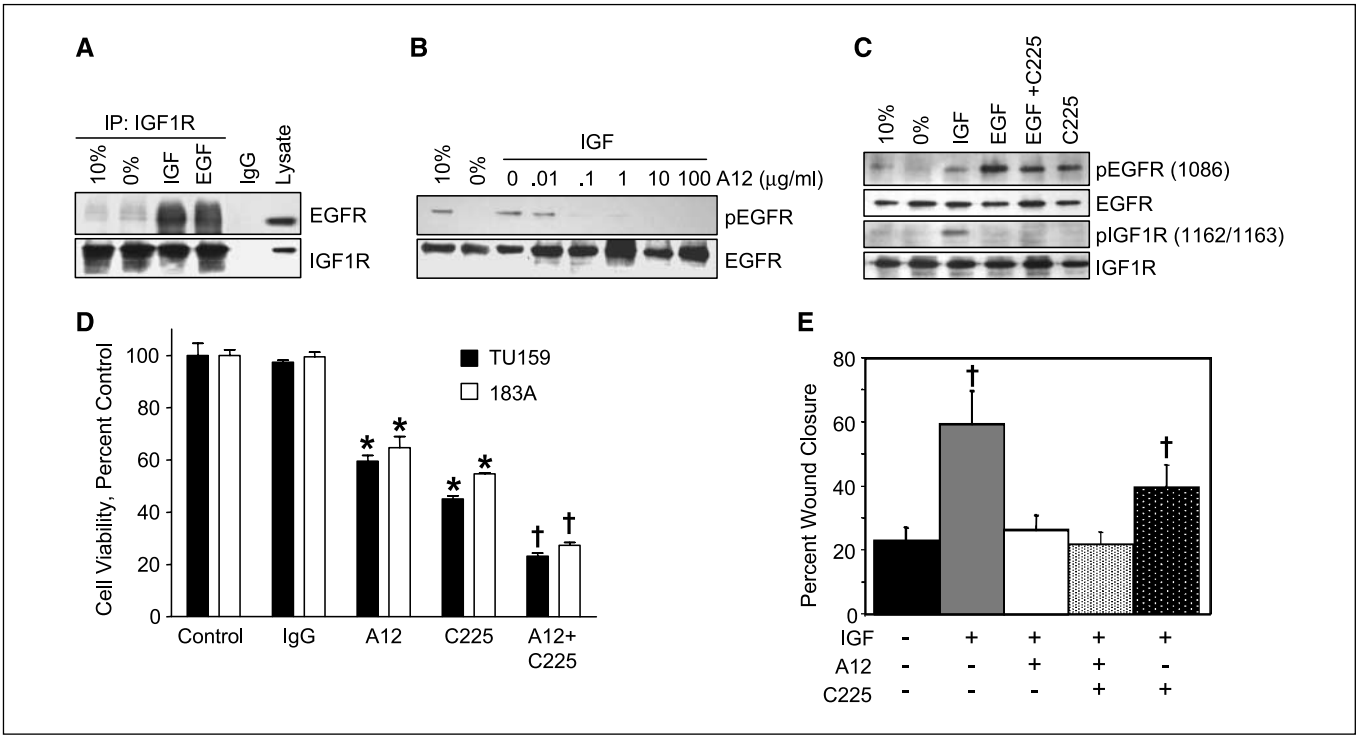

Fig. 5. IGF-IR and EGFR interaction in SCCHN cells. *A,* TU159 cells were grown in medium with 10% FCS or 0% FCS +/- IGF (10 ng/mL) or EGF (10 ng/mL) stimulation for 10 min. Cells were then lysed, proteins immunoprecipitated with an anti – IGF-IR antibody, and protein detected by Western blot. *B,* TU159 cells were treated as described, then analyzed by Western blot for phospho-Y1086 EGFR or total EGFR protein. *C,* TU159 cells were treated as described, then analyzed by Western blot for the indicated phosphorylated or total proteins with specific antibodies (IGF, 10 ng/mL; EGF, 10 ng/mL; C225, 100 nmol/L). *D,* cell viability was assessed by 3-(4,5-dimethylthiazol-2-yl)-2,5-diphenyltetrazolium bromide assay in TU159 and 183A SCCHN cells grown in medium with 10% FCS and treated with nothing (control), immunoglobulin G (10 μg/mL), A12 (10 μg/mL), C225 (100 nmol/L), or A12 + C225, for 48 h. Control cell values were normalized to 100%. Columns, mean of four independent experiments; bars, SD. *E,* TU159 cells were grown to confluency, wounded, and then incubated with IGF alone or IGF plus A12, C225, or A12 + C225 for 24 h. Each plate was examined by phase-contrast microscopy for the amount of wound closure. Ten separate measurements were made per plate and each experiment was done in triplicate. Columns, mean of three experiments; bars, SD. * and †, $P < 0.05$, different from control group and from all other groups, respectively.

tumors were treated thrice a week for 4 weeks with i.p. injections of vehicle, A12, C225, or both A12 and C225 at doses that had proved effective in other model systems (23, 24, 36–39). Weight gain during initial tumor growth and during treatment was not significantly different between the treatment groups (data not shown), providing one indication that no significant systemic morbidity had occurred. These results are similar to those reported when prostate cancer xenografts were successfully treated with A12 (24).

Treatment with A12, C225, or the combination all caused negative tumor growth slopes that were significantly different from that of the control group by linear regression analysis (Fig. 6A). In the A12 treatment group, 13 of 16 tumors showed either no change or a decrease in volume, with five tumors that completely regressed (Fig. 6B). C225 alone was also quite effective, with all tumors showing either no growth (1 of 16), regression (10 of 16), or complete regression (5 of 16). Results were similar for the combination treatment group, with only one tumor that increased in volume during the 4-week treatment period and 7 of 16 (44%) of tumors that completely regressed. This the first report of the potential therapeutic efficacy of either A12 or C225 against human tongue cancer xenografts. The doses chosen were so effective in this model system that a possible additive or synergistic benefit to combining these two agents could not be shown with the current data set. One explanation for C225 efficacy in this model system is that C225 has been reported to show enhanced antitumor activity in PTEN-deficient cancer cells (40). However, mounting data from other cancer types imply that combining A12 and C225 may prove more effective than single agents and at lower doses, decreasing the risk of treatment-related side effects and possibly overcoming tumor resistance to anti-EGFR therapies (32, 34, 41). Future experiments are planned to address this issue.

Finally, it is interesting to note that there were significant differences in tumor histology between the different treatment groups. Specifically, the control group and C225-treated tumors showed moderate to poor differentiation with significant areas of necrosis, whereas the A12 and A12 plus C225 treatment groups displayed significant squamous differentiation with elongated, flattened cells and numerous keratin pearls (Fig. 6C). Immunohistochemical analysis for the proliferation marker PCNA showed that there is a significant decrease in the staining intensity of PCNA in A12- and C225-treated groups as compared with control. The decrease in PCNA is much more pronounced in A12 + C225–treated group (Fig. 6C, *right*). IGF-IR signaling has been reported to inhibit normal squamous differentiation of keratinocytes and tissue organization in *in vitro* skin models (42); thus, inhibition of IGF-IR through A12 therapy may actually be causing the TU159 cell line to differentiate. Thus, in addition to the potential for combinations of A12 and C225 to more effectively reduce or eliminate

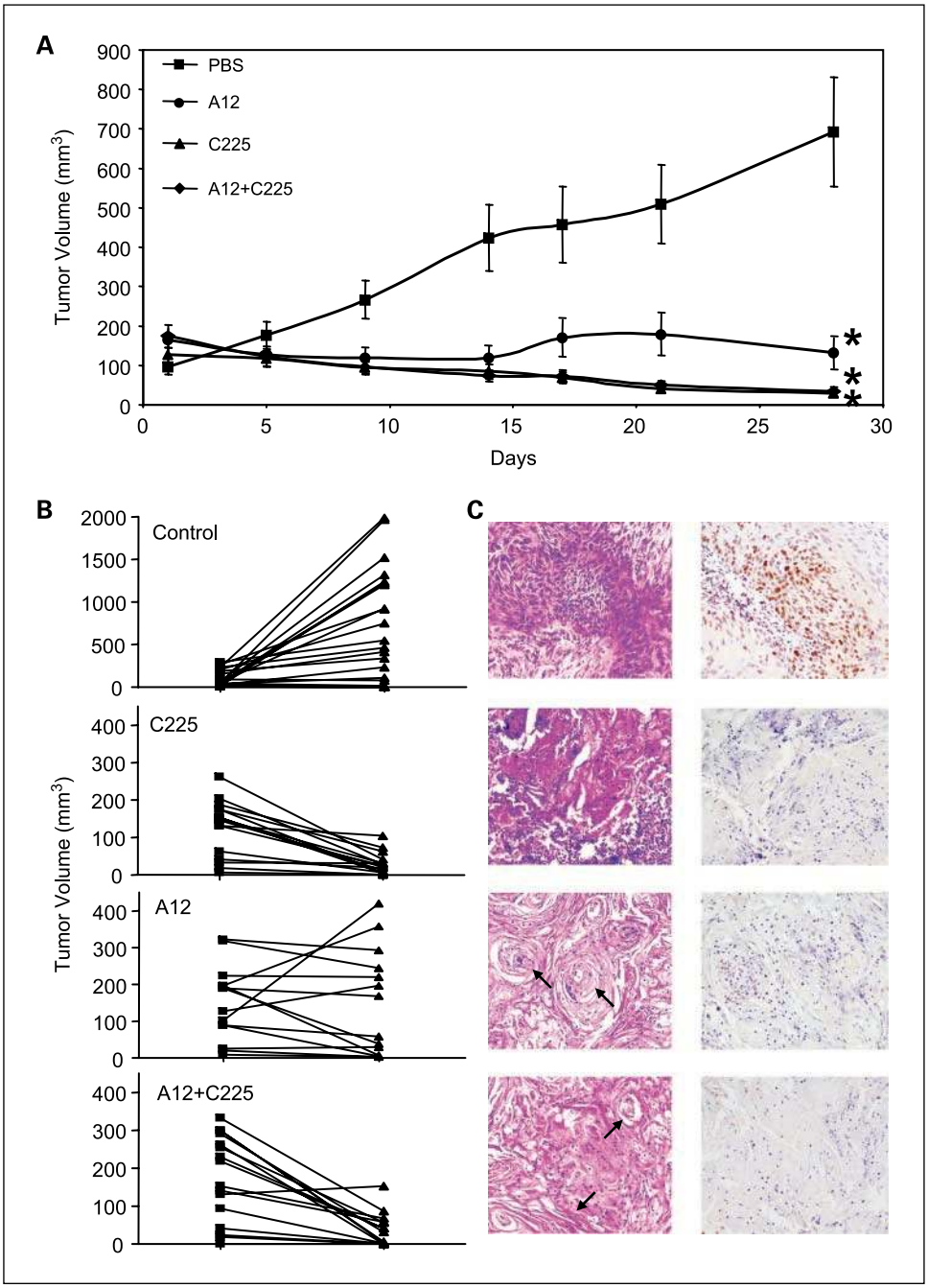

Fig. 6. Inhibition of SCCHN xenograft growth by A12 and C225. *A,* TU159 cells (1×10^6) s.c. injected in each hind flank of athymic nude mice. Mice with established tumors (100-200 mm^3) received equal-volume i.p. injections of PBS, A12 (40 mg/kg), C225 (40 mg/kg), or both A12 and C225 (40 mg/kg each) thrice a week for 4 wks. Points, mean tumor volumes assessed for each group, graphed versus time; bars, SD. *, $P < 0.05$, significantly different slope of growth curve versus PBS group. *B,* tumor volumes at the start and end of treatment are plotted to display individual tumor trends per group. *C,* representative photomicrographs of H&E-stained tumor sections at ×10 magnification (*left*). Arrows, elongated, flattened cells and keratin pearls. Immunohistochemical analysis of these sections for the proliferation marker PCNA showed that there is a significant decrease in the staining intensity of PCNA in A12- and C225-treated groups as compared with control. The decrease in PCNA is much more pronounced in A12 + C225–treated group (*right*).

tumor burden with fewer C225-induced treatment-related side effects, A12 may provide the additional benefit of inducing squamous differentiation in remaining tumor cells. In many cases, complete removal of head and neck tumors either causes significant morbidity or is not possible due to complicated tumor presentation and local tissue invasion. Through A12-induced differentiation of any remaining tumor burden, this potential new therapy may decrease the possibility of tumor recurrence or of second primary tumors in this disease. However, it will also be important to carefully evaluate the safety and possible unique side effects of anti–IGF-IR therapies because down-regulation of the insulin receptor has been reported with anti–IGF-IR antibodies (43). Likewise, IGF-IR is virtually ubiquitously expressed and blockade of IGF-IR may have systemic negative effects, particularly in tissues with rapid turnover, the cardiovascular system and the peripheral nervous system (44).

In conclusion, we have shown here for the first time that IGF-IR expression is increased in human head and neck cancer and that IGF-IR signaling significantly influences the proliferation, motility, and tumorigenicity of human head and neck cancer cell lines. We have also shown that EGFR and IGF-IR functionally heterodimerize in this disease and have provided a basis for combined anti-receptor tyrosine kinase directed therapies. These novel findings justify the further exploration of targeting IGF-IR as a new therapeutic strategy against head and neck cancer.

References

1. Chin D, Boyle GM, Porceddu S, Theile DR, Parsons PG, Coman WB. Head and neck cancer: past, present and future. Exp Rev Anticancer Ther 2006;6:1111 – 8.

2. Lothaire P, de Azambuja E, Dequanter D, et al. Molecular markers of head and neck squamous cell carcinoma: promising signs in need of prospective evaluation. Head Neck 2006;28:256 – 69.

3. Modjtahedi H. Molecular therapy of head and neck cancer. Cancer Metastasis Rev 2005;24:129 – 46.

4. Pollak MN, Schernhammer ES, Hankinson SE. Insulin-like growth factors and neoplasia. Nat Rev Cancer 2004;4:505 – 18.

5. Mitsiades CS, Mitsiades N. Treatment of hematologic malignancies and solid tumors by inhibiting IGF receptor signaling. Expert Rev Anticancer Ther 2005;5: 487 – 99.

6. Larsson O, Girnita A, Girnita L. Role of insulin-like growth factor 1 receptor signalling in cancer. Br J Cancer 2005;92:2097 – 101.

7. Reinmuth N, Fan F, Liu W, et al. Impact of insulin-like growth factor receptor-I function on angiogenesis, growth, and metastasis of colon cancer. Lab Invest 2002;82:1377 – 89.

8. Zeng H, Datta K, Neid M, Li J, Parangi S, Mukhopadhyay D. Requirement of different signaling pathways mediated by insulin-like growth factor-I receptor for proliferation, invasion, and VPF/VEGF expression in a pancreatic carcinoma cell line. Biochem Biophys Res Commun 2003;302:46 – 55.

9. Zhang X, Lin M, van Golen KL, Yoshioka K, Itoh K, Yee D. Multiple signaling pathways are activated during insulin-like growth factor-I (IGF-I) stimulated breast cancer cell migration. Breast Cancer Res Treat 2005; 93:159 – 68.

10. Carboni JM, Lee AV, Hadsell DL, et al. Tumor development by transgenic expression of a constitutively active insulin-like growth factor I receptor. Cancer Res 2005;65:3781 – 7.

11. Sell C, Dumenil G, Deveaud C, et al. Effect of a null mutation of the insulin-like growth factor I receptor gene on growth and transformation of mouse embryo fibroblasts. Mol Cell Biol 1994;14:3604 – 12.

12. Vincent AM, Feldman EL. Control of cell survival by IGF signaling pathways. Growth Horm IGF Res 2002; 12:193 – 7.

13. Clemmons DR, Maile LA. Minireview: Integral membrane proteins that function coordinately with the insulin-like growth factor I receptor to regulate intracellular signaling. Endocrinology 2003;144: 1664 – 70.

14. Sachdev D, Hartell JS, Lee AV, Zhang X, Yee D. A dominant negative type I insulin-like growth factor receptor inhibits metastasis of human cancer cells. J Biol Chem 2004;279:5017 – 24.

15. Goel HL, Breen M, Zhang J, et al. β1A integrin expression is required for type 1 insulin-like growth factor receptor mitogenic and transforming activities and localization to focal contacts. Cancer Res 2005;65: 6692 – 700.

16. Beckhardt RN, Kiyokawa N, Xi L, et al. HER-2/neu oncogene characterization in head and neck squamous cell carcinoma. Arch Otolaryngol Head Neck Surg 1995;121:1265 – 70.

17. Yang Z, Barnes CJ, Kumar R. Human epidermal growth factor receptor 2 status modulates subcellular localization of and interaction with estrogen receptor α in breast cancer cells. Clin Cancer Res 2004;10: 3621 – 8.

18. Acconcia F, Barnes CJ, Kumar R. Estrogen and tamoxifen induce cytoskeletal remodeling and migration in endometrial cancer cells. Endocrinology 2006;147: 1203 – 12.

19. Sells MA, Pfaff A, Chernoff J. Temporal and spatial distribution of activated Pak1 in fibroblasts. J Cell Biol 2002;151:1449 – 58.

20. Vadlamudi RK, Adam L, Wang RA, et al. Regulatable expression of p21-activated kinase-1 promotes anchorage-independent growth and abnormal organization of mitotic spindles in human epithelial breast cancer cells. J Biol Chem 2000;2750:36238 – 440.

21. Zhang H, Yee D. The therapeutic potential of agents targeting the type I insulin-like growth factor receptor. Expert Opin Investig Drugs 2004;13:1569 – 77.

22. Hofmann F, Garcia-Echeverria C. Blocking insulin-like growth factor-I receptor as a strategy for targeting cancer. Drug Discov Today 2005;10:1041 – 7.

23. Lu D, Zhang HF, Koo H, et al. A fully human recombinant IgG-like bispecific antibody to both the epidermal growth factor receptor and the insulin-like growth factor receptor for enhanced antitumor activity. J Biol Chem 2005;280:19665 – 72.

24. Wu JD, Odman A, Higgins LM, et al. *In vivo* effects of the human type I insulin-like growth factor receptor antibody A12 on androgen-dependent and androgen-independent xenograft human prostate tumors. Clin Cancer Res 2005;11:3065 – 74.

25. Burtrum D, Zhu Z, Lu D, et al. A fully human monoclonal antibody to the insulin-like growth factor I receptor blocks ligand-dependent signaling and inhibits human tumor growth *in vivo*. Cancer Res 2003;63: 8912 – 21.

26. Poetsch M, Lorenz G, Kleist B. Detection of new PTEN/MMAC1 mutations in head and neck squamous cell carcinomas with loss of chromosome 10. Cancer Genet Cytogenet 2002;132:20 – 4.

27. Pedrero JM, Carracedo DG, Pinto CM, et al. Frequent genetic and biochemical alterations of the PI 3-K/AKT/PTEN pathway in head and neck squamous cell carcinoma. Int J Cancer 2005;114:242 – 8.

28. Segrelles C, Moral M, Lara MF, et al. Molecular determinants of Akt-induced keratinocyte transformation. Oncogene 2006;25:1174 – 85.

29. Groner B, Hartmann C, Wels W. Therapeutic antibodies. Curr Mol Med 2004;4:539 – 47.

30. Balda MS, Matter K. Epithelial cell adhesion and the regulation of gene expression. Trends Cell Biol 2003; 13:310 – 8.

31. Adams TE, McKern NM, Ward CW. Signalling by the type 1 insulin-like growth factor receptor: interplay with the epidermal growth factor receptor. Growth Factors 2004;22:89 – 95.

32. Chakravarti A, Loeffler JS, Dyson NJ. Insulin-like growth factor receptor I mediates resistance to anti-epidermal growth factor receptor therapy in primary human glioblastoma cells through continued activation of phosphoinositide 3-kinase signaling. Cancer Res 2002;62:200 – 7.

33. Jones HE, Goddard L, Gee JM, et al. Insulin-like growth factor-I receptor signalling and acquired resistance to gefitinib (ZD1839; Iressa) in human breast and prostate cancer cells. Endocr Relat Cancer 2004; 11:793 – 814.

34. Ueda S, Hatsuse K, Tsuda H, et al. Potential cross-talk between insulin-like growth factor receptor type 1 and epidermal growth factor receptor in progression and metastasis of pancreatic cancer. Mod Pathol 2006;19:788 – 96.

35. Thelemann A, Petti F, Griffin G, et al. Phosphotyrosine signaling networks in epidermal growth factor receptor overexpressing squamous carcinoma cells. Mol Cell Proteomics 2005;4:356 – 76.

36. Huang SM, Li J, Harari PM. Molecular inhibition of angiogenesis and metastatic potential in human squamous cell carcinomas after epidermal growth factor receptor blockade. Mol Cancer Ther 2002;1:507 – 14.

37. Prewett MC, Hooper AT, Bassi R, Ellis LM, Waksal HW, Hicklin DJ. Enhanced antitumor activity of anti-epidermal growth factor receptor monoclonal antibody IMC-C225 in combination with irinotecan (CPT-11) against human colorectal tumor xenografts. Clin Cancer Res 2002;8:994 – 1003.

38. Overholser JP, Prewett MC, Hooper AT, Waksal HW, Hicklin DJ. Epidermal growth factor receptor blockade by antibody IMC-C225 inhibits growth of a human pancreatic carcinoma xenograft in nude mice. Cancer 2000;89:74 – 82.

39. Prewett M, Rothman M, Waksal H, Feldman M, Bander NH, Hicklin DJ. Mouse-human chimeric anti-epidermal growth factor receptor antibody C225 inhibits the growth of human renal cell carcinoma xenografts in nude mice. Clin Cancer Res 1998;4: 2957 – 66.

40. Li X, Luwor R, Lu Y, Liang K, Fan Z. Enhancement of antitumor activity of the anti-EGF receptor monoclonal antibody cetuximab/C225 by perifosine in PTEN-deficient cancer cells. Oncogene 2006;25: 525 – 35.

41. Knowlden JM, Hutcheson IR, Barrow D, Gee JM, Nicholson RI. Insulin-like growth factor-I receptor signaling in tamoxifen-resistant breast cancer: a supporting role to the epidermal growth factor receptor. Endocrinology 2005;146:4609 – 18.

42. Sadagurski M, Yakar S, Weingarten G, et al. Insulin-like growth factor 1 receptor signaling regulates skin development and inhibits skin keratinocyte differentiation. Mol Cell Biol 2006;26:2675 – 87.

43. Sachdev D, Singh R, Fujita-Yamaguchi Y, Yee D. Down-regulation of insulin receptor by antibodies against the type I insulin-like growth factor receptor: implications for anti-insulin-like growth factor therapy in breast cancer. Cancer Res 2006;66:2391 – 402.

44. Miller BS, Yee D. Type I insulin-like growth factor receptor as a therapeutic target in cancer. Cancer Res 2005;65:10123 – 7.

Clinical Cancer Research

Insulin-like Growth Factor Receptor as a Therapeutic Target in Head and Neck Cancer

Christopher J. Barnes, Kazufumi Ohshiro, Suresh K. Rayala, et al.

Clin Cancer Res 2007;13:4291-4299.